

Testing the relationship between the Llewellyn fault, Tally-Ho shear zone, and gold mineralization in northwest British Columbia



Luke Ootes^{1, a}, Sébastien Castonguay², Richard Friedman³, Fionnuala Devine⁴, and Reid Simmonds⁵

¹ British Columbia Geological Survey, Ministry of Energy, Mines and Petroleum Resources, Victoria, BC, V8W 9N3

² Geological Survey of Canada, Natural Resources Canada, Quebec City, QC, G1K 9A9

³ Pacific Centre for Geochemical and Isotopic Research, University of British Columbia, Vancouver, BC, V6T 1Z4

⁴ Merlin Geosciences Inc., Atlin, BC, V0W 1A0

⁵ School of Earth and Ocean Sciences, University of Victoria, Victoria, BC, V8P 5C2

^a corresponding author: Luke.Ootes@gov.bc.ca

Recommended citation: Ootes, L., Castonguay, S., Friedman, R., Devine, F., and Simmonds, R., 2018. Testing the relationship between the Llewellyn fault, Tally-Ho shear zone, and gold mineralization in northwest British Columbia. In: Geological Fieldwork 2017, British Columbia Ministry of Energy, Mines and Petroleum Resources, British Columbia Geological Survey Paper 2018-1, pp. 67-81.

Abstract

The Llewellyn fault represents a significant geological feature in northwest British Columbia. The fault is a southeast-striking, steeply dipping brittle dextral strike-slip structure that overprints 'early' ductile deformation, which is preserved as foliations, lineations, and folds in the host rocks. The Tally-Ho shear zone, Yukon, shares similar early ductile deformation and is overprinted by the Llewellyn fault. In general, the deformation corridor demarcates the eastern limit of metamorphic suites (Triassic and older rocks of the Nisling terrane and Boundary Ranges metamorphic suite) and the western limit of the younger Stuhini (Triassic) and Laberge (Jurassic) groups. Previous work and this study demonstrate that brittle strike-slip deformation along the Llewellyn fault occurred between ca. 56 and 50 Ma. New field observations indicate the early ductile deformation is represented by one foliation (S_{main}) along the Llewellyn fault and Tally-Ho shear zone corridor. Two granodiorite intrusions crosscut the early deformation features, and new U-Pb zircon chemical abrasion ID-TIMS results indicate they crystallized at ca. 75 Ma. In the Tally-Ho shear zone, the S_{main} is parallel to a foliation in an adjacent granodiorite, mapped as part of the Whitehorse plutonic complex (ca. 120 Ma). In British Columbia, a deformed rhyolite along the Llewellyn fault yielded a preliminary ca. 120 Ma age. Based on these results, we infer that the early ductile fabrics formed before ca. 75 Ma and, potentially, after ca. 120 Ma.

A goal of this study was to establish if the early ductile and late brittle structures represent a crustal-scale, ductile-brittle deformation continuum. If so, could various gold mineralization styles (epithermal, mesothermal, intrusion-related) along the structural corridor be related in time and be part of an orogenic gold mineralizing system? This study demonstrates that, although the early ductile and late brittle deformation share the same space, they developed at least ca. 20 Ma apart and are not part of a structural continuum. This result indicates the various styles of gold mineralization developed during temporally distinct tectonic events.

Keywords: Llewellyn fault, Tally-Ho shear zone, U-Pb geochronology, gold

1. Introduction

This study was designed to document the geologic setting and controls of gold mineralization spatially associated with selected major fault zones of the Canadian Cordillera. The chosen field laboratory extends from the Tagish Lake area of northwest British Columbia northward to the Wheaton River area in southern Yukon (Fig. 1). This area is the locus of a series of vein-hosted gold prospects and deposits, including past-producing mines (e.g., Engineer, Mount Skukum) that are spatially related to the Llewellyn fault and Tally-Ho shear zone (e.g., Hart and Radloff, 1990; Mihalynuk et al., 1999; Tizzard et al., 2009; Ootes et al., 2017). The area also encompasses multiple lithotectonic suites that are affected by the faults (Fig. 2). The timing of deformation along the fault zones and the temporal and genetic relationships with intrusion-related,

mesothermal, and epithermal-style gold systems remain to be clearly established.

Herein we present new field observations about the relationship between the Llewellyn fault and the Tally-Ho shear zone (Hart and Radloff, 1990; Tizzard et al., 2009) and five new chemical abrasion ID-TIMS U-Pb zircon ages. These data constrain the timing of ductile and the late brittle strain and associated gold mineralization that characterizes this deformation corridor.

2. Background and geology

The Llewellyn fault extends along strike northwest from British Columbia to the Tally-Ho shear zone in Yukon (Figs. 1, 2). In general, this deformation zone marks the boundary between the Nisling terrane to the west and Stikine

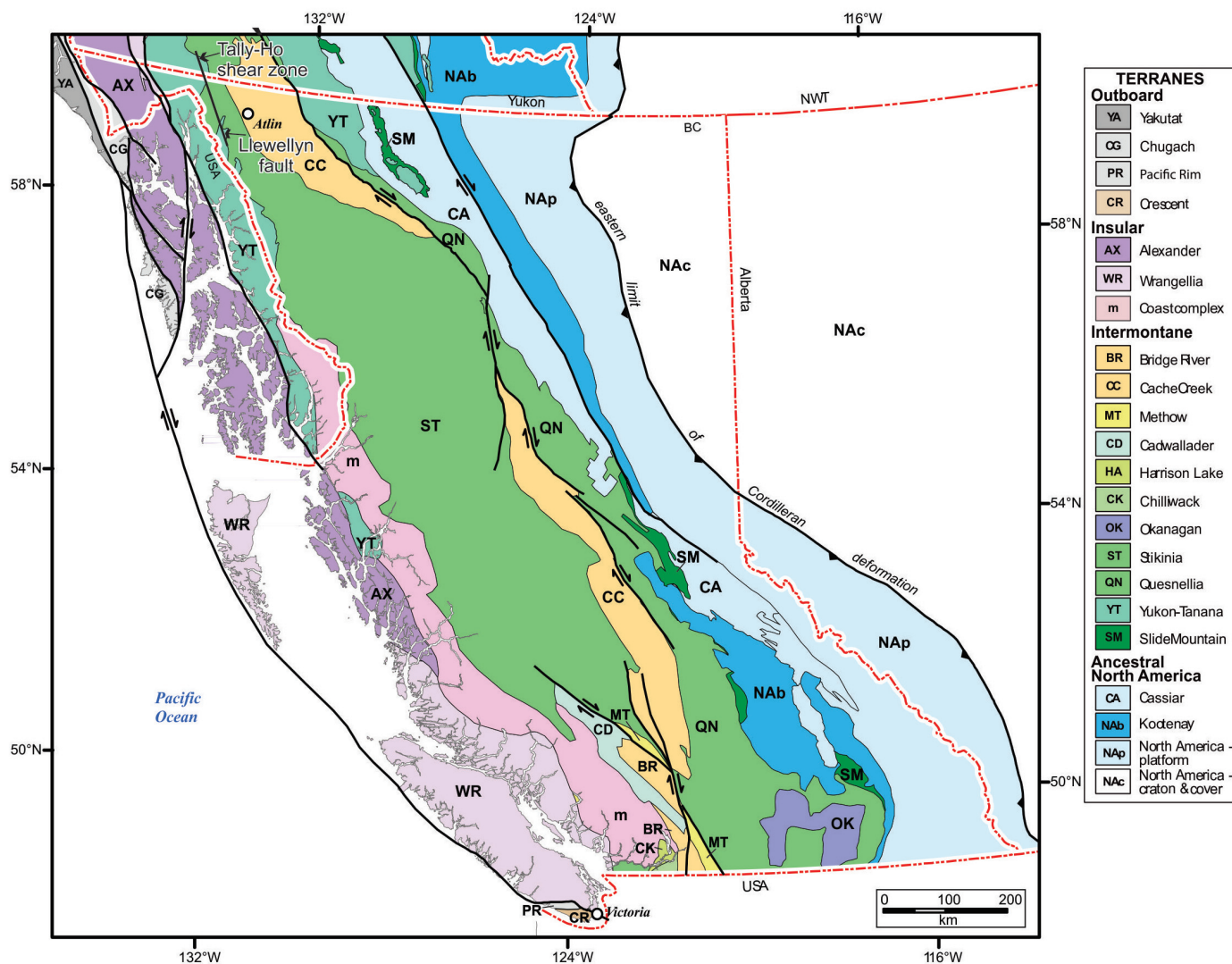


Fig. 1. Terrane map of British Columbia and neighbouring jurisdictions. Modified after Nelson et al. (2013).

terrane to the east (Fig. 2; Hart and Radloff, 1990; Mihalynuk et al., 1999) and is spatially associated with a variety of gold prospects and minor past producers (Fig. 2). This gold mineralization has characteristics that range from mesothermal (Montana Mountain mines; Fig. 2; Roots, 1981; Walton, 1986; Hart and Pelletier, 1989), to epithermal (Mount Skukum and Engineer mines; Love, 1990, Love et al., 1998; Millinog et al., 2017), to intrusion-related (Bennett plateau and Middle ridge prospects, Golden Eagle project; Mihalynuk et al., 2003; Wark, 2012).

Reconnaissance fieldwork, data compilation, and preliminary reports (Castonguay et al., 2017; Ootes et al., 2017) have underlined that the epithermal gold mineralization at the Engineer and Mount Skukum deposits coincide both spatially and temporally with Eocene magmatism (also see Love et al., 1998; Millinog et al., 2017). These first-order observations led to the suggestion of a relationship between large-scale deformation zones, gold mineralization, and Eocene magmatism in southwest Yukon and northwest British Columbia.

2.1. Tally-Ho shear zone

2.1.1. Overview

North of the BC-Yukon border, the Tally-Ho shear zone is defined by a corridor of strongly deformed amphibolite, marble, and schist, assigned to the Povoas Formation of the Lewes River Group (Upper Triassic; equivalent to Stuhini Group in British Columbia). This corridor is bounded on either side by younger intrusions (Fig. 2; Doherty and Hart, 1988; Hart and Radloff, 1990; Tizzard et al., 2009). The shear zone can be traced for ~40 km along strike and is best exposed between Tally-Ho Mountain and Mount Hodnett (Hart and Radloff, 1990; Tizzard et al., 2009). The shear zone comprises marbles and amphibolites that have a southwest-dipping penetrative foliation to mylonitic fabric, and a shallow southeast- or northwest-plunging mineral lineation (Fig. 3; Hart and Radloff, 1990). Bedding is locally preserved in marble layers, but is strongly transposed into the foliation as the mylonite zones are approached (Hart and Radloff, 1990; Tizzard et al., 2009).

Hart and Radloff (1990) interpreted that the Tally-Ho shear

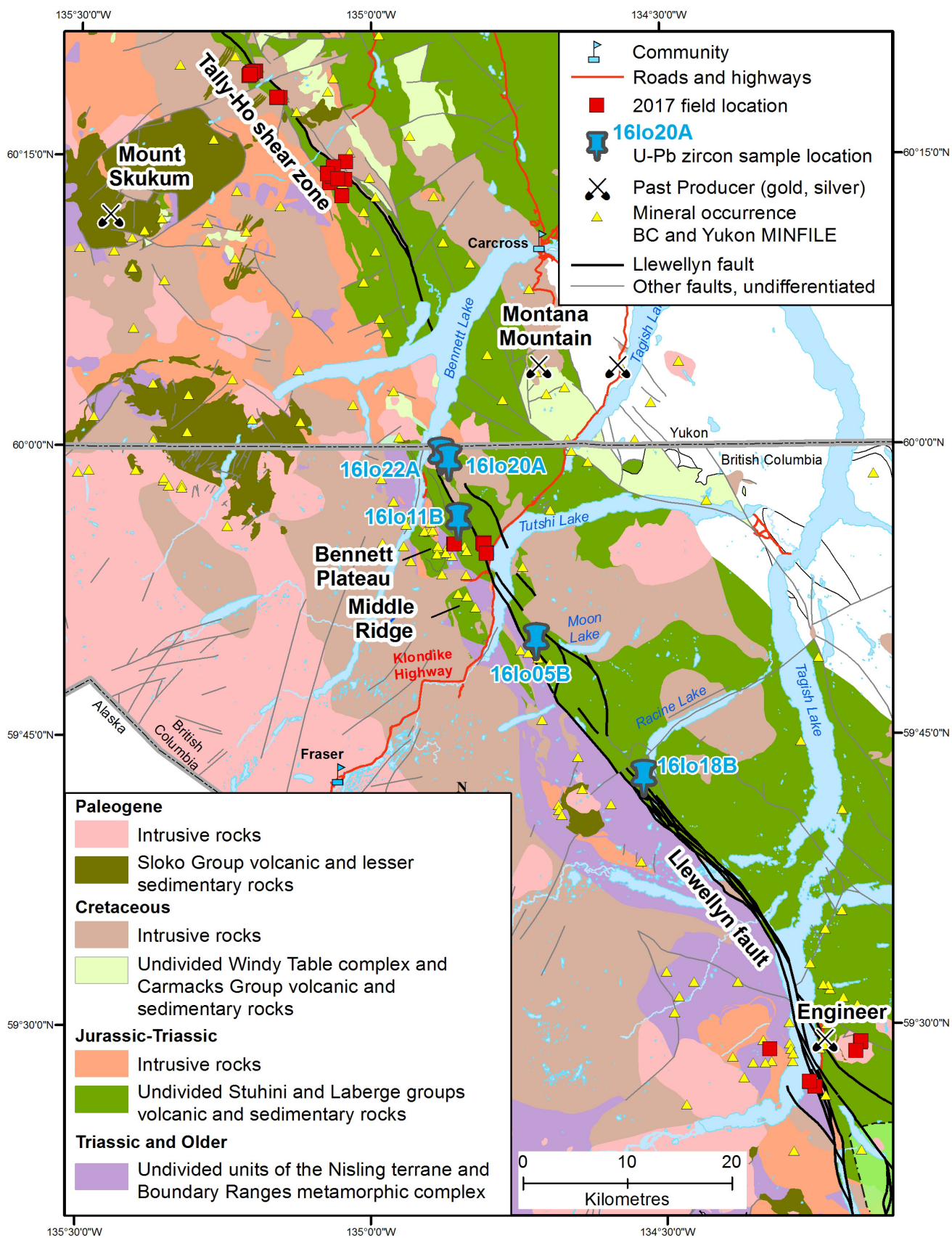


Fig. 2. Simplified geology near the Llewellyn fault and Tally-Ho shear zone. Geology is after Doherty and Hart (1988), Hart and Pelletier (1989), Hart and Radloff (1990), and Mihalyuk et al. (1999). Rocks of the Cache Creek assemblage (upper right) are unfilled.

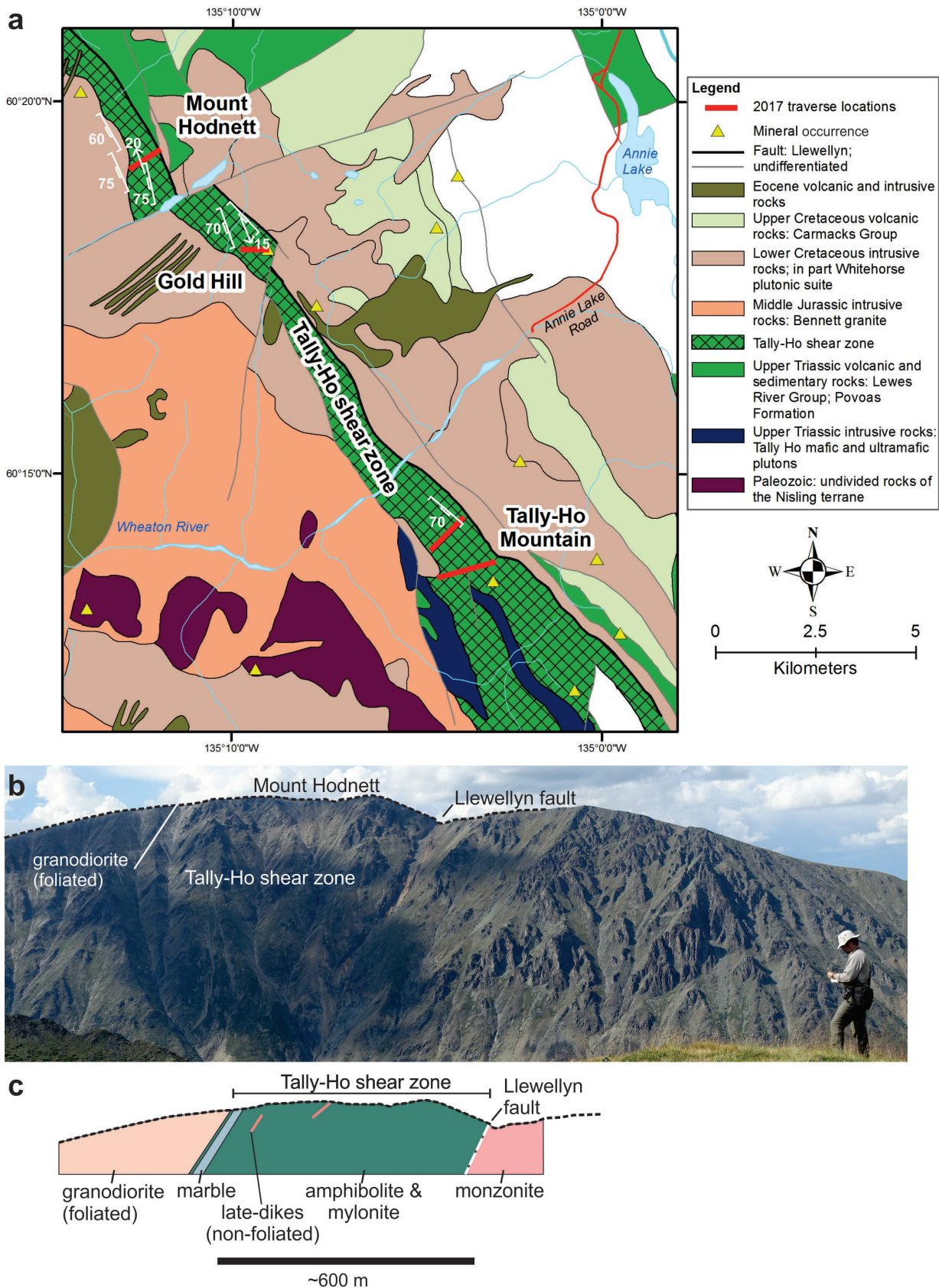


Fig. 3. a) Simplified geology of the Tally-Ho shear zone, southern Yukon (modified after Hart and Radloff, 1990). Generalized foliations (line with pendants) and lineations (arrows) are from this study and Hart and Radloff (1990). **b)** View of Mount Hodnett and Tally-Ho shear zone from Gold Hill. View is north. **c)** Geological sketch of Mount Hodnett, in upper left of photo; in part modified after Tizzard et al. (2009).

zone records predominantly sinistral deformation between 230 and 220 Ma, and speculated on its potential importance as a terrane-bounding thrust fault. Revising this interpretation, Tizzard et al. (2009) considered that the shear zone represents a top-to-the-east crustal thrust fault that was later folded during Nisling-Stikine collision. Accordingly, foliated gabbro and pyroxenite (hangingwall) were thrust over Povoas Formation (shear zone and footwall) and subsequently affected by upright folds (Tizzard et al., 2009). Uranium-lead zircon ages of ca. 208 Ma for leucogabbro in the hangingwall and ca. 173 Ma for undeformed K-feldspar porphyritic granite west of the shear zone bracket the timing of thrusting and subsequent folding (Tizzard et al., 2009).

Brittle deformation features are parallel to and overprint the Tally-Ho shear zone ductile fabrics. These include faults with dextral offset and fractures (Hart and Radloff (1990). Hart and Radloff (1990) mapped one particular brittle fault zone along the east side of the Tally-Ho shear zone, which they correlated to the Llewellyn fault (Figs. 2, 3).

2.1.2. Field observations

Traverses across the Tally-Ho shear zone were conducted in the Tally-Ho Mountain, Gold Hill, and Mount Hodnett areas of Yukon (Figs. 2, 3). The best exposed and accessible section appears to be at Mount Hodnett (Fig. 3). Exposed units include (from west to east): weakly to moderately foliated granodiorite in sheared contact with steeply west-dipping amphibolite and marble; strongly sheared mafic volcanoclastic rocks (mylonite); and foliated metabasalt (Figs. 3 and 4). Bedding (S_0) is preserved and folded in the marble. Folds have shallow northwest, or southeast plunging axes and axial planes are parallel to the main foliation (S_{main} ; Fig. 4a). The S_{main} occurs in all rocks but is best developed in mylonitic volcanoclastic beds, where the composite layering may be a result of S_{main} being parallel to S_0 (Fig. 4b). East of this, the shear zone is mostly strongly foliated (S_{main}) amphibolite/metabasalt (Fig. 4c). Kinematic indicators, albeit rare, include shear bands, sigmoidal porphyroclasts, and quartz vein boudins, suggest apparent northeast-directed motion. However, the shallowly plunging stretching and/or mineral lineation on S_{main} indicates strike-slip movement. Locally, the older ductile fabrics are offset and kinked along discrete brittle faults. Along the eastern side of the shear zone the foliated amphibolite/metabasalt is structurally interlayered with moderately foliated monzonite (Fig. 3c). This juxtaposition is the result of sub-vertical brittle high strain zones marked by cataclasite that overprints the foliation in the metabasalt (Figs. 3, 4d). This brittle fault zone is <10 m wide and consists of cataclasite and carbonate alteration. Drill collars attest that the zones have been tested by exploration drilling. All units are intruded by unfoliated feldspar-porphyritic intermediate dikes (Fig. 4d).

The granodiorite west of the shear zone (Fig. 3a) was assigned to the Whitehorse plutonic suite (ca. 120 Ma; Hart and Radloff, 1990). This granodiorite contains a foliation, defined by biotite and hornblende that are now partially altered to chlorite. This

foliation strikes south-southeast and dips west ($165^\circ/70^\circ\text{W}$) and is parallel to the S_{main} in the deformation zone (ca. $170^\circ/75^\circ\text{W}$; Figs. 3, 4). Because only one foliation has been identified in the shear zone (Fig. 4), it is best interpreted as having been derived from the same deformation (also see Hart and Radloff, 1990).

2.2. Llewellyn fault

2.2.1. Overview

The Llewellyn fault is a southeast-striking, steeply dipping brittle dextral strike-slip structure that overprints early ductile fabrics. The structure continues for >100 km, from the Tulsequah area in the south to beyond the BC-Yukon border in the north (Mihalynuk et al., 1994, 1999). The Llewellyn fault represents a domain boundary (Fig. 2), with the Boundary Ranges metamorphic suite to the west (pre-Triassic; part of Stikine or Nisling terrane?) and Stuhini and Laberge group volcano-sedimentary rocks to the east (Triassic-Jurassic; part of the Stikine Terrane; Fig. 2; Mihalynuk et al., 1999). Along the Llewellyn structure, the rocks contain penetrative fabrics (folds, foliations, and lineations) that trend south-southeast, and have been interpreted to indicate sinistral shear (Mihalynuk et al., 1999). The ductile deformation post-dates deposition of the Laberge Group (Jurassic). Older deformation fabrics may occur in pre-Triassic rocks (e.g., Boundary Ranges metamorphic complex), but the subparallel nature of the fabrics along the Llewellyn fault precludes subdivision (e.g., Mihalynuk et al., 1999). Upper Cretaceous and Eocene plutons crosscut the ductile fabrics, providing a minimum age for the ductile deformation (Mihalynuk et al., 1999).

Brittle deformation along the Llewellyn fault is temporally constrained by vein-hosted gold mineralization at Engineer Mine. There, vanadian illite, produced by fluid-rock interaction during epithermal vein formation, has been dated by ^{40}Ar - ^{39}Ar at ca. 50 Ma (Millonig et al., 2017). As the epithermal veins at Engineer are related to brittle deformation along the Llewellyn fault, this age approximates the timing of brittle strike-slip movement (e.g., Ootes et al., 2016; Millonig et al., 2017). This timing coincides with Cordillera-wide dextral strike-slip faulting (e.g., Gabrielse et al., 2006).

2.2.2. Field observations

Some locations along the Llewellyn fault, previously investigated by Ootes et al. (2017), were revisited in 2017. In the Bennett plateau and Tagish Lake areas, British Columbia, traverses were conducted across the Llewellyn fault zone (Figs. 2, 3). At Bennett plateau, the 'Skarn zone' (Fig. 2) is known to host gold and base-metal mineralization that developed with a series of hydrothermal quartz-actinolite veins hosted in metasedimentary rocks of the Stuhini Group (Fig. 5; Mihalynuk et al., 1999; Wark, 2012). These veins are boudinaged and folded (z-shaped; Figs. 5a, b). Where identifiable, bedding and foliation strike northwest and dip steeply to moderately east (ca. $345^\circ/50^\circ\text{E}$). A 2 m-wide porphyry intrusion with a fine-grained siliceous matrix and quartz-feldspar-biotite phenocrysts (granodiorite) intruded

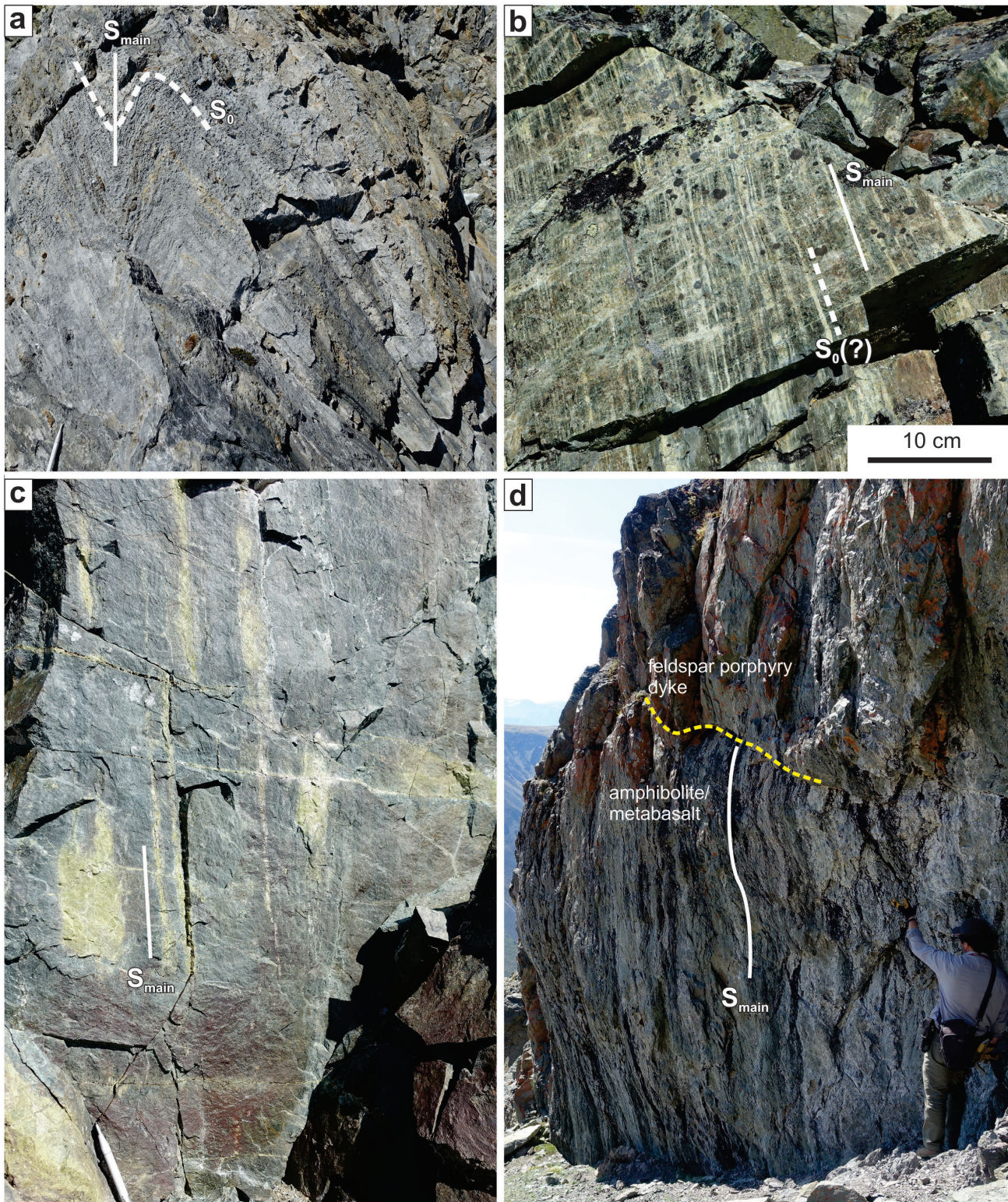


Fig. 4. Tally-Ho shear zone, Mount Hodnett. **a)** Povoas Formation marble, with folded bedding (S_0) and subvertical axial trace (S_{main}). View is to the north and folds plunge gently northward, and parallel locally developed mineral lineations. Scribe for scale (bottom left) is 13 cm long. **b)** Volcaniclastic unit 5 m east of the marble. S_0 and S_{main} form a composite layering. This unit has been interpreted as a mylonite (Hart and Radloff, 1990; Tizzard et al., 2009). View is north. **c)** Typical amphibolite unit in the shear zone, with S_{main} defined by aligned alteration pods defined by epidote. Scribe for scale (bottom left). View is south. **d)** Recessive-weathering cataclasite zone where brittle fault intersects the foliated amphibolite. The rock face represents the intersection of the amphibolite and the fault plane and person is standing on the cataclasite zone. The top half of the outcrop is a massive, intermediate feldspar-porphyry dike that intruded after ductile deformation but is caught in the brittle fault. View is southwest.

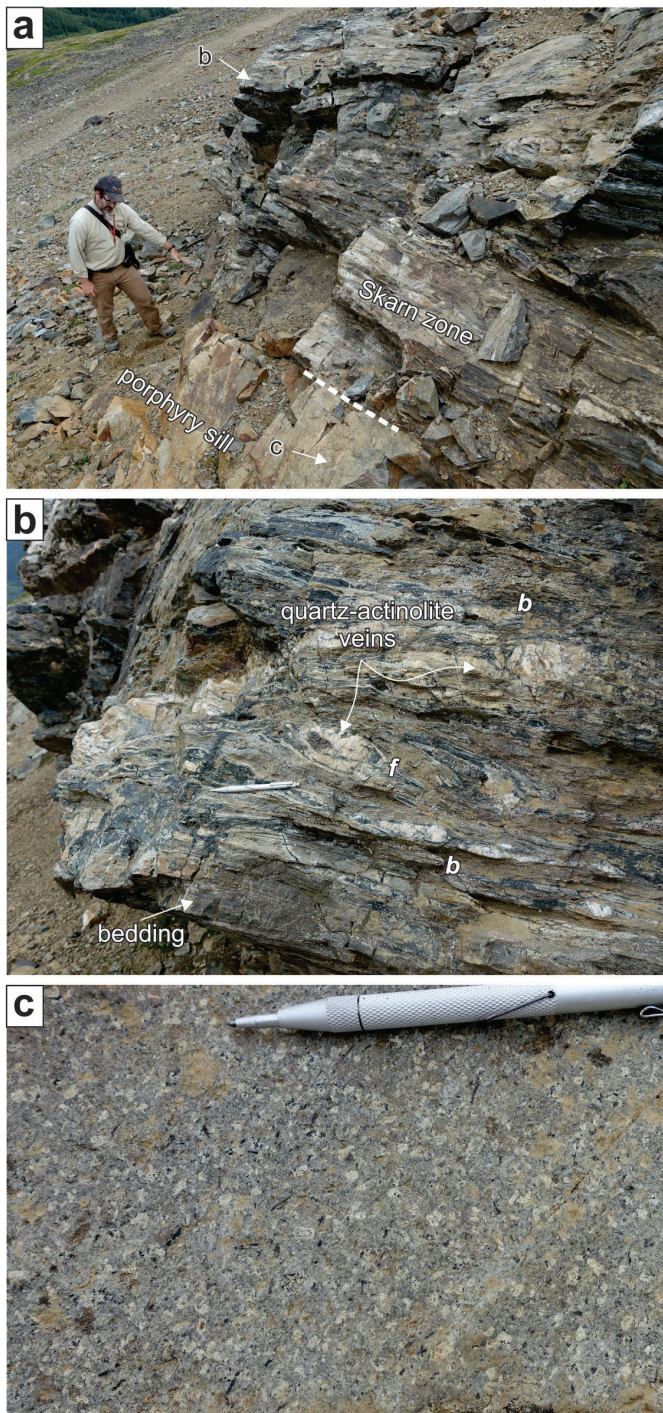


Fig. 5. **a)** Typical exposure of the Skarn zone near Bennett plateau, where a porphyry sill intruded previously deformed metasedimentary rocks of the Stuhini Group that host hydrothermal quartz-actinolite veins. View is northeast. **b)** Example of folded (*f*) and boudinaged (*b*) quartz-actinolite veins in metasedimentary rocks in the Skarn zone. Scribe for scale (bottom left) is 13 cm long. View is east. **c)** Weathered surface of post-deformation granodiorite porphyry sill. A sample of this sill was collected for U-Pb zircon geochronology (sample 16lo11B) and yielded an age of 76.30 ± 0.05 Ma.

the Skarn zone (Figs. 5a, c). The granodiorite post-dates deformation but the intrusive contact is parallel to the fabrics in the host-rock (Fig. 5a).

A composite gneiss, assigned to the Boundary Ranges metamorphic suite, outcrops immediately west of the Llewellyn fault near the Wann River at the south end of Tagish Lake (Figs. 6a, b; Mihalyuk et al., 1999). The gneiss is a mixed unit of diorite to granite, with local garnet-amphibolite representing boudinaged mafic dikes, or enclaves (Fig. 6b). Intrusive relationships are complicated by the strong structural overprint, defined by a foliation in massive rock types (e.g., granite) and gneissic layering (Fig. 6b). Veins, ca. 5 cm wide, are defined by quartz crystals with long axes perpendicular to vein margins (Fig. 6b). These veins belong to a spectrum of syn- to post- S_{main} shear and extensional structures.

Between 100 and 500 m southeast and directly along strike of these quartz veins are the vein-hosted showings Lum/Wann (Au-Ag-Cu-Pb-Zn; MINFILE 104M 109) and Brown (Ag-Au-Cu-Pb-Zn-Mo; MINFILE 104M 026). Approximately 750 m to the south, within dense bush cover, is float with tetrahedrite-bearing quartz veins (presumed to be the Brownie showing; Fig. 6c). This float is derived from weathering of an adjacent cliff face, but the remainder of the veins are in subcrop. Based on preliminary observations, these veins appear to be parallel to layering, presumably S_{main} in the host rocks.

3. U-Pb zircon geochronology

To further test the timing of deformation along the Llewellyn fault, in 2016 we collected samples for U-Pb geochronology from five separate sites along the strike of the fault where contact relationships are well exposed (Fig. 2). Additional samples, collected in 2017, are being processed.

3.1. CA-ID-TIMS analytical techniques

The U-Pb zircon chemical abrasion isotope dilution thermal ionization mass spectrometry (CA-ID-TIMS) procedures described here are modified from Mundil et al. (2004), Mattinson (2005), and Scoates and Friedman (2008). After rock samples underwent standard mineral separation procedures, the zircons were handpicked in alcohol. The clearest, crack- and inclusion-free grains are selected, photographed, and then annealed in quartz glass crucibles at 900°C for 60 hours. Annealed grains were transferred into 3.5 mL PFA screwtop beakers, ultrapure HF (up to 50% strength, 500 mL) and HNO_3 (up to 14 N, 50 mL) were added, and caps closed finger tight. The beakers were placed in 125 mL PTFE liners (up to four per liner) and about 2 mL HF and 0.2 mL HNO_3 of the same strength as acid in the beakers containing the samples were added to the liners. The liners were then slid into stainless steel Parr™ high-pressure dissolution devices, sealed, and heated to a maximum of 200°C for 8-16 hours (typically 190°C for 12 hours). Beakers were removed from the liners and the zircon separated from leachate. Zircons were rinsed with >18 M Ω .cm water and subboiled acetone. Then, 2 mL of subboiled 6N HCl was added and the beakers set on a hotplate at 80° - 130°C

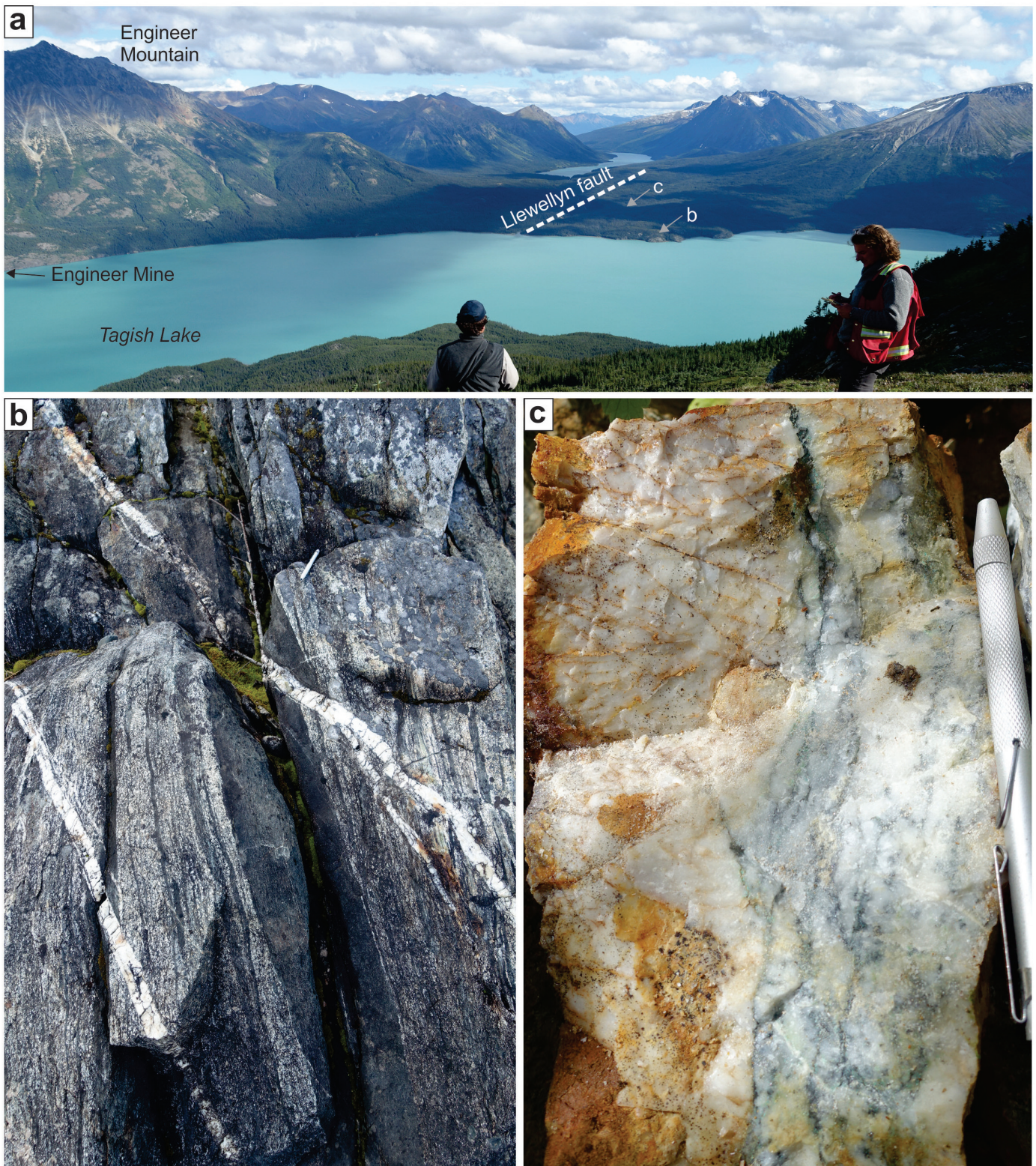


Fig. 6. a) Panoramic view of the trace of the Llewellyn fault at the south end of Tagish Lake. Mount Engineer is an Eocene volcanic complex. Locations of photographs in b) and c) are indicated. View is southeast. **b)** Mixed gneiss of the Boundary Ranges metamorphic suite, immediately west of the Llewellyn fault at the south end of Tagish Lake. The gneiss has felsic and mafic protoliths. Quartz veins, with quartz with long axes normal to vein margins, appear to post-date the main foliation, but are part of a spectrum of syn- to post-deformation. **c)** Hydrothermal quartz-carbonate vein with laminated metallic mineralization (tetrahedrite) at the Brownie prospect. The sample is in float and it likely eroded from adjacent till-blanketed escarpment. Preliminary results (n=5) indicate the veins carry a range of precious and base-metals: Au (200 to 8300 ppb); Ag (140 to 360 ppm); Cu (1100 to 8200 ppm); Pb (2650 to >5000 ppm); Zn (1800 to 4950 ppm); and Hg (2800 to 9600 ppm). Location is ~750 m south of Tagish Lake.

for 30 minutes and, again, rinsed with water and acetone. Masses were estimated from the dimensions (volumes) of grains. Single zircon grains were transferred into clean 300 mL PFA microcapsules (crucibles), and 50 mL 50% HF and 5 mL 14 N HNO₃ was added. Each was then spiked with a ²³³⁻²³⁵U-²⁰⁵Pb tracer solution (EARTHTIME ET535), capped, and again placed in a Parr liner (8-15 microcapsules per liner). HF and nitric acids in a 10:1 ratio, respectively, were added to the liner, which was then placed in a Parr high-pressure device and dissolution achieved at 220°C for 40 hours. The resulting solutions were dried on a hotplate at 130°C, and 50 mL 6N HCl was added to microcapsules and fluorides dissolved in high-pressure Parr devices for 12 hours at 180°C. HCl solutions were transferred into clean 7 mL PFA beakers and dried with 2 mL of 0.5 N H₃PO₄. Samples were loaded onto degassed, zone-refined Re filaments in 2 mL of silicic acid emitter (Gerstenberger and Haase, 1997).

Isotopic ratios were measured with a single collector VG Sector 54 thermal ionization mass spectrometer equipped with analogue Daly photomultiplier. Analytical blanks are 0.1 pg for U and up to 1.1 pg for Pb. U fractionation was determined directly on individual runs using the EARTHTIME ET535 mixed ²³³⁻²³⁵U-²⁰⁵Pb isotopic tracer and Pb isotopic ratios were corrected for fractionation of 0.25 ± 0.04%/amu, based on replicate analyses of NBS-982 reference material and the values recommended by Thirlwall (2000). Data reduction employed the Excel-based program of Schmitz and Schoene (2007). Standard concordia diagrams were constructed and regression intercepts and weighted averages calculated with Isoplot (Ludwig, 2003). Unless otherwise noted, all errors are quoted at 2σ (95% level of confidence). Isotopic ages are calculated with the decay constants $\lambda_{238} = 1.55125E-10$ and $\lambda_{235} = 9.8485E-10$ (Jaffey et al., 1971) and a ²³⁸U/²³⁵U ratio of 137.88. EARTHTIME U-Pb synthetic solutions were analyzed on an on-going basis to monitor the accuracy of results.

3.2. Results

3.2.1. K-feldspar porphyritic granite (sample #16lo20A)

A sample was collected from a medium-grained granite with k-feldspar phenocrysts from east of the Llewellyn fault and south of the BC-Yukon border (Fig. 2). The granite pluton intruded foliated Laberge Group metasedimentary rocks and was mapped as middle Cretaceous to Tertiary (unit LKqm in Mihalynuk et al., 1999). The granite does not contain a foliation or display evidence of brittle faulting. Five prismatic grains selected from the zircon separates yield three overlapping concordant results and two slightly older, marginally concordant to slightly discordant results (Fig. 7a; Table 1). A ²⁰⁶Pb/²³⁸U weighted mean of the three youngest overlapping concordant results yield an age of 56.58 ± 0.07 Ma, interpreted as the crystallization age of the granite. Two results that are marginally concordant to slightly discordant have ²⁰⁶Pb/²³⁸U ages only 100 Ka (±2σ) older than the weighted mean and are interpreted as antecrysts (Fig. 7a; Table 1).

3.2.2. Equigranular granite (sample #16lo22A)

Equigranular biotite-hornblende granite was collected from east of Bennett Lake and south of the British Columbia-Yukon border (Fig. 2). The granite was mapped as a middle Cretaceous to Tertiary pluton and interpreted to crosscut both ductile and brittle Llewellyn structures (unit LKgl in Mihalynuk et al., 1999; Pennington pluton discussed in Hart and Radloff, 1990). The granite lacks a ductile fabric, but contains closely spaced (<30 cm) brittle fractures, striking 360° and dipping 65°E, directly along strike of the Llewellyn fault (Fig. 2) and probably related to the fault. The sample yielded prismatic igneous zircon and five single grains were selected for analysis by CA-ID-TIMS. The results overlap on concordia and a ²⁰⁶Pb/²³⁸U weighted mean of four of the five results yields a crystallization age of 56.46 ± 0.06 Ma. One result is slightly older (56.75 Ma) and interpreted as an antecryst (Fig. 7b; Table 1).

3.2.3. Granodiorite porphyry (16lo11B)

A 2 m-wide quartz-, feldspar-, and biotite-phyric intrusion with a fine-grained siliceous matrix (granodiorite porphyry) intrudes metasedimentary rocks of the Stuhini Group at Bennett plateau (Figs. 2 and 5). The metasedimentary rocks contain hydrothermal quartz-actinolite veins that were folded and boudinaged, and the area that contains these veins has been termed the Skarn zone. The granodiorite intrusion parallels the host rock fabrics, but post-dates the ductile deformation (Fig. 5). A sample of the granodiorite porphyry yielded good-quality igneous zircons. Four zircons were selected for analysis and yield overlapping, concordant results. A ²⁰⁶Pb/²³⁸U weighted mean age of 76.30 ± 0.05 Ma is interpreted as the crystallization of the intrusion (Fig. 7c; Table 1).

3.2.4. Granodiorite (sample #16lo05B)

West of Moon Lake, within the trace of the Llewellyn fault, a fine- to medium-grained, weakly porphyritic (~0.5 cm-wide feldspar) granodiorite (unit Mgd in Mihalynuk et al., 1999), with moderate carbonate alteration and partially chloritized biotite and hornblende, cuts across the contact between the Stuhini Group and the Boundary Ranges metamorphic suite. The eastern contact of the granodiorite is parallel to bedding and foliation in Stuhini Group argillite; the granodiorite lacks a foliation and post-dates the ductile deformation preserved in the host argillite. The granodiorite is crosscut by a southeast-striking brittle fault, identifiable in the outcrop as a 2 m-wide zone of fault gouge with intense fracturing and carbonate alteration (see Figure 4a in Ootes et al., 2017). We collected a sample of least-altered granodiorite from near the contact with the host argillite.

The sample yielded good-quality igneous zircon and five single grains were selected for analysis. The results are concordant to slightly discordant and have a range of ²⁰⁶Pb/²³⁸U ages, from ca. 92 Ma to 74 Ma (Fig. 7d; Table 1). The youngest zircon, at ca. 74 Ma, gives the best estimate for the time of crystallization of the granodiorite sample. Older zircons with marginally concordant to discordant results and ²⁰⁶Pb/²³⁸U dates

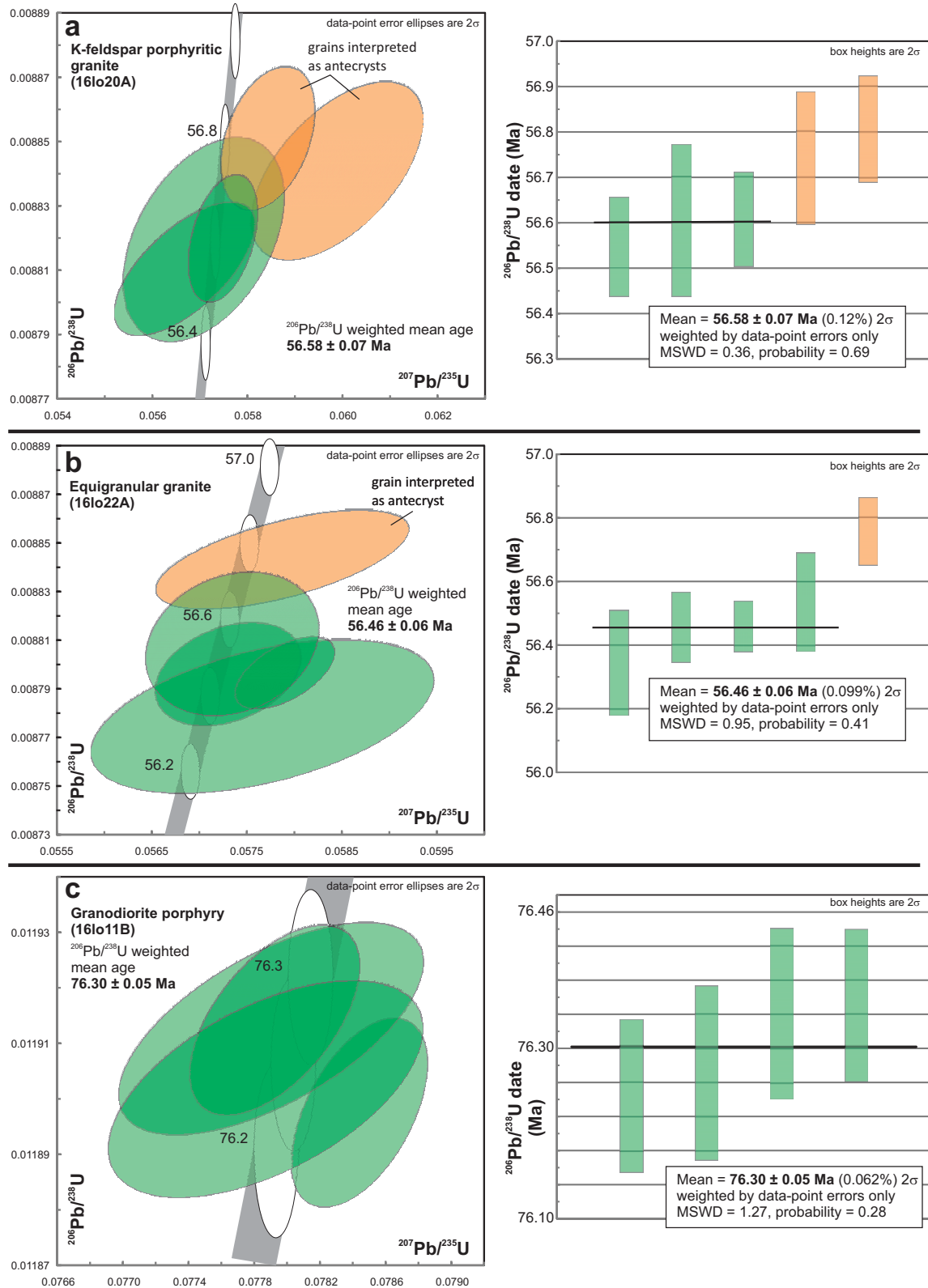


Fig. 7. Results of chemical abrasion ID-TIMS U-Pb zircon geochronology. **a-b)** K-feldspar phenocrystic granite and equigranular granite (Bennett granite) from east of Bennett Lake and south of the BC-Yukon border. **c)** Granodiorite porphyry from the Skarn zone, Bennett plateau. In figures a-c) Concordia plot is on the left and corresponding weighted mean diagram is on the right. Green ellipses and bars indicate results used in age determinations; orange ellipses and bars indicate results not used in age determinations. MSWD=mean square of weighted deviates. Sample locations are in Figure 2, analytical results are in Table 1.

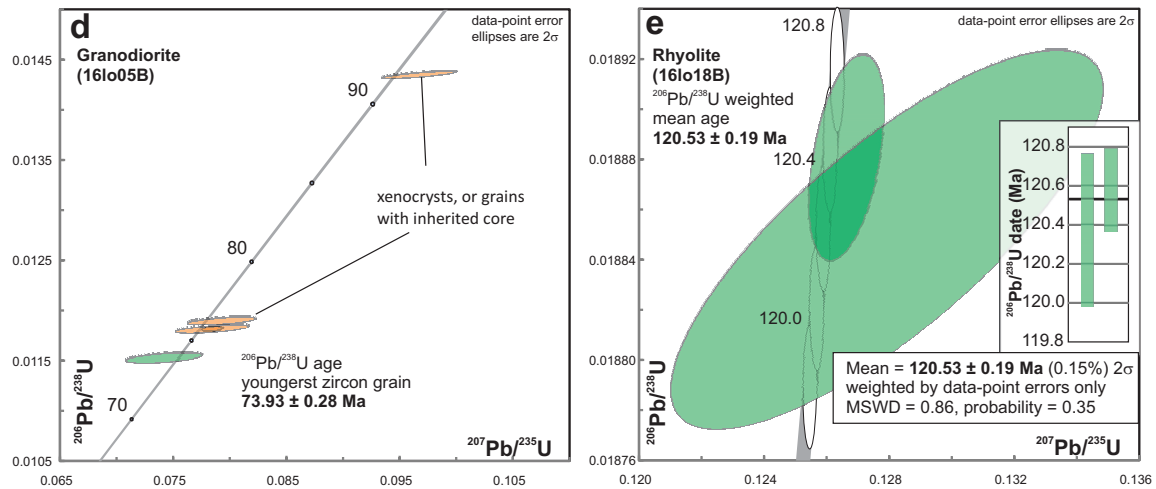


Fig. 7 continued. Results of chemical abrasion ID-TIMS U-Pb zircon geochronology. **d)** Granodiorite samples from west of Moon Lake. **e)** Rhyolite from west of Racine Lake; inset is the weighted mean of the two zircons analyzed. Green ellipses and bars indicate results used in age determinations; orange ellipses and bars indicate results not used in age determinations. MSWD=mean square of weighted deviates. Sample locations are in Figure 2, analytical results are in Table 1.

of ca. 76 Ma ($n=3$) and ca. 90 Ma are interpreted as xenocrysts, or as composite grains with older inherited cores and younger rims (Fig. 7d).

3.2.5. Rhyolite (161o18B)

Southwest of Racine Lake and directly east of Teepee Peak is a zone of imbricated Stuhini Group and minor Laberge Group rocks (Mihalynuk et al., 1999). The best exposures are on a hummock-like ridge that is transected by the brittle Llewellyn fault and related splays. The western-most splay separates Stuhini and Laberge group from Boundary Ranges metamorphic suite rocks (Mihalynuk et al., 1999). Outcrops along the ridge contain a ridge-parallel foliation ($\sim 135^\circ/80^\circ\text{SW}$) that is locally affected by steeply plunging minor folds (s-shaped). The rock types in the west are predominantly argillite and in the east black shale (slate) and marble. An intermediary unit of 'rhyolite' and associated rocks was identified by Mihalynuk et al. (1999) and during this study. The rhyolite unit weathers chalky white and contains plagioclase and quartz phenocrysts and is commonly moderately to strongly foliated, consistent with the other units on the outcrop. The rhyolite is also carbonate altered, potentially related to brittle faulting along this zone. A sample of massive rhyolite with carbonate alteration was selected for geochronology. Only two of six zircons survived the journey from separation to mass spectrometry but yield overlapping and concordant U/Pb ages. A $^{206}\text{Pb}/^{238}\text{U}$ weighted mean of the analyses indicate a crystallization age of ca. 121 Ma (Fig. 7e; Table 1).

4. Discussion

4.1. Timing of deformation

The new U-Pb geochronology allows the timing of deformation along the Llewellyn fault to be bracketed. The crystallization age for the granodiorite pluton west of Moon Lake

(161o05b) is ca. 74 Ma; the age for the granodiorite porphyry sill on Bennett plateau (161o11b) is 76 Ma (Figs. 7d, e). Both of these intrusions post-date ductile deformation in the Stuhini and Laberge groups and Boundary Ranges metamorphic suite. Therefore ductile deformation pre-dates 76-74 Ma. The granodiorite west of Moon Lake is crosscut by the brittle Llewellyn fault, constraining the brittle deformation to younger than ca. 74 Ma.

Near the BC-Yukon border, two granitic plutons sampled for this study (161o20a, 161o22a; Fig. 2) yield indistinguishable ages of ca. 56.5 and 56.6 Ma (Figs. 7a, b). Both intrusive phases post-date ductile deformation. The slightly older K-feldspar porphyritic granite lacks evidence of brittle deformation. However, the slightly younger equigranular granite pluton (161o20a) contains fractures that are along strike, and parallel to, the brittle fault trace, although these fractures contain neither carbonate alteration nor fault gouge such as along the Llewellyn fault to the south (e.g., see Figure 4 in Ootes et al., 2017). Thus, either brittle deformation was protracted and the granite records the latest in a long movement history or, given that the pluton is relatively homogenous, it acted as a rigid body during brittle movement and was only fractured. We favour the latter interpretation because the fractures in the granite ($360/65^\circ\text{E}$) are directly in line with the fault trace. Brittle deformation continued after the granite intruded, as indicated by ^{40}Ar - ^{39}Ar dating of vanadinite from Engineer Mine (~ 70 km to the southeast, Fig. 2), which indicates brittle movement and associated epithermal veining along the fault at ca. 50 Ma (Millonig et al., 2017). In addition, epithermal quartz veins at Mount Skukum (~ 40 km to the northwest) are related to regional strike-slip brittle faults, and these veins and associated alteration have been dated at ca. 54 Ma (Love et al., 1998). This timing (Fig. 8) is coeval with Cordilleran-scale brittle dextral strike-slip faulting (e.g., Gabrielse et al., 2006). It does remain

Table 1. Results of chemical abrasion ID-TIMS U-Pb zircon geochronology.

Sample (a)	Compositional Parameters										Radiogenic Isotope Ratios						Isotopic Ages							
	Wt. mg	U ppm	Pb ppm	Th U	$^{206}\text{Pb}^*$ $\times 10^{-13}$ mol	mol % $^{206}\text{Pb}^*$	Pb* Pb _c	^{206}Pb ^{204}Pb	^{208}Pb ^{206}Pb	^{207}Pb ^{206}Pb	% err	^{238}U ^{206}Pb	% err	^{235}U ^{206}Pb	% err	^{238}U ^{206}Pb	^{207}Pb ^{206}Pb	^{235}U ^{206}Pb	^{238}U ^{206}Pb	\pm	\pm	\pm	\pm	
16lo20A - K-feldspar porphyritic granite (*507641m E, 6647497m N)																								
A	0.004	292	2.7	0.385	0.4415	98.64%	21	0.50	1365	0.124	0.04912	2.331	0.05988	2.467	0.00884	0.257	0.568	154	55	59.0	1.4	56.74	0.15	
B	0.005	229	2.1	0.353	0.4213	98.45%	18	0.55	1194	0.113	0.04694	2.301	0.05708	2.408	0.00882	0.295	0.417	46	55	56.4	1.3	56.61	0.17	
C	0.005	327	3.0	0.365	0.5791	98.93%	27	0.51	1739	0.117	0.04788	1.308	0.05843	1.372	0.00885	0.206	0.377	93	31	57.66	0.77	56.81	0.12	
D	0.004	244	2.3	0.339	0.3319	97.91%	14	0.58	888	0.109	0.04666	1.997	0.05668	2.119	0.00881	0.193	0.661	32	48	56.0	1.2	56.55	0.11	
E	0.006	484	4.4	0.370	0.9796	99.00%	29	0.82	1847	0.119	0.04727	0.969	0.05749	1.026	0.00882	0.184	0.392	63	23	56.8	0.6	56.61	0.10	
16lo22B - equigranular granite (*507270m E, 6649185m N)																								
A	0.0112	266	2.4	0.382	1.0967	99.32%	43	0.61	2739	0.122	0.04725	1.040	0.05731	1.087	0.00880	0.197	0.324	62	25	56.58	0.60	56.46	0.11	
B	0.0046	333	3.1	0.377	0.5599	98.71%	22	0.60	1430	0.121	0.04764	2.431	0.05767	2.555	0.00878	0.294	0.469	82	58	56.9	1.4	56.35	0.17	
C	0.0066	152	1.4	0.418	0.3701	98.40%	18	0.49	1160	0.134	0.04747	1.769	0.05788	1.878	0.00884	0.188	0.613	73	42	57.1	1.0	56.76	0.11	
D	0.0055	461	4.2	0.422	0.9323	99.36%	46	0.50	2877	0.135	0.04774	0.669	0.05790	0.738	0.00880	0.139	0.570	86	16	57.15	0.41	56.46	0.08	
E	0.0096	219	2.0	0.384	0.7763	99.16%	35	0.54	2210	0.123	0.04722	1.267	0.05735	1.294	0.00881	0.275	0.205	60	30	56.62	0.71	56.54	0.16	
16lo11B - granodiorite porphyry (*507977m E, 6642004m N)																								
A	0.0082	320	4.0	0.499	1.3073	99.34%	46	0.71	2803	0.160	0.04782	0.383	0.07844	0.430	0.01190	0.117	0.516	90.2	9.1	76.68	0.32	76.24	0.09	
B	0.0029	384	4.9	0.495	0.5606	99.05%	32	0.44	1950	0.159	0.04743	0.895	0.07790	0.971	0.01191	0.131	0.625	71	21	76.17	0.71	76.34	0.10	
C	0.0040	362	4.5	0.460	0.7124	99.19%	37	0.48	2279	0.147	0.04744	0.485	0.07793	0.542	0.01191	0.117	0.567	71	12	76.19	0.40	76.35	0.09	
E	0.0036	201	2.6	0.469	0.3576	98.59%	21	0.42	1311	0.150	0.04745	0.937	0.07787	1.004	0.01190	0.135	0.552	72	22	76.14	0.74	76.27	0.10	
16lo05B - granodiorite (*515870m E, 6630703m N)																								
A	0.0079	103	1.3	0.519	0.3933	97.85%	14	0.71	861	0.166	0.04669	3.536	0.07425	3.718	0.01153	0.379	0.519	33	85	72.7	2.6	73.93	0.28	
B	0.0220	31	0.5	0.396	0.4148	98.47%	19	0.53	1210	0.127	0.04890	2.618	0.09677	2.792	0.01435	0.223	0.796	143	61	93.8	2.5	91.86	0.20	
C	0.0055	94	1.3	0.654	0.2581	98.19%	17	0.39	1019	0.210	0.04836	2.888	0.07937	3.051	0.01190	0.291	0.592	117	68	77.6	2.3	76.28	0.22	
D	0.0153	97	1.2	0.542	0.7300	99.39%	50	0.37	3012	0.174	0.04817	0.896	0.07854	0.961	0.01183	0.184	0.436	108	21	76.77	0.71	75.78	0.14	
E	0.0091	113	1.5	0.534	0.5046	97.59%	12	1.03	767	0.171	0.04816	3.169	0.07850	3.356	0.01182	0.316	0.621	107	75	76.7	2.5	75.76	0.24	
16lo18B - deformed and altered rhyolite (*526116m E, 6617833m N)																								
B	0.0172	113	2.3	0.532	1.5266	99.20%	38	1.01	2317	0.170	0.04864	0.715	0.12663	0.773	0.01888	0.178	0.431	131	17	121.07	0.88	120.58	0.21	
C	0.0014	120	3.2	0.607	0.1303	90.72%	3	1.10	199	0.194	0.04922	4.142	0.12792	4.397	0.01885	0.328	0.791	158	97	122.2	5.1	120.37	0.39	

(a) A, B etc. are labels for fractions composed of single zircon grains or fragments; all fractions annealed and chemically abraded after Mattinson (2005) and Scoates and Friedman (2008).

(b) Nominal fraction weights estimated from photomicrographic grain dimensions, adjusted for partial dissolution and chemical abrasion.

(c) Nominal U and total Pb concentrations subject to uncertainty in photomicrographic estimation of weight and partial dissolution during chemical abrasion.

(d) Model Th/U ratio calculated from radiogenic $^{208}\text{Pb}/^{206}\text{Pb}$ ratio and $^{207}\text{Pb}/^{235}\text{U}$ age.

(e) Pb* and Pb_c represent radiogenic and common Pb, respectively; mol % $^{206}\text{Pb}^*$ with respect to radiogenic, blank and initial common Pb.

(f) Measured ratio corrected for spike and fractionation only. Mass discrimination of $0.25 \pm 0.04\%$ amu based on analysis of NBS-982; all Daly analyses.

(g) Corrected for fractionation, spike and all common Pb assumed to be procedural blank: $^{206}\text{Pb}/^{204}\text{Pb} = 18.50 \pm 1.0\%$, $^{207}\text{Pb}/^{204}\text{Pb} = 15.50 \pm 1.0\%$, $^{208}\text{Pb}/^{204}\text{Pb} = 38.40 \pm 1.0\%$ (all uncertainties 1-sigma).

(h) Errors are 2-sigma, propagated using the algorithms of Schmitz and Schoene (2007) and Crowley et al. (2007).

(i) Calculations are based on the decay constants of Jaffey et al. (1971). $^{238}\text{U}/^{235}\text{U} = 137.88$, $^{206}\text{Pb}/^{238}\text{U}$ and $^{207}\text{Pb}/^{206}\text{Pb}$ ages corrected for initial disequilibrium in $^{230}\text{Th}/^{238}\text{U}$ using Th/U [magma] = 3.

*UTM Zone 8, NAD 83

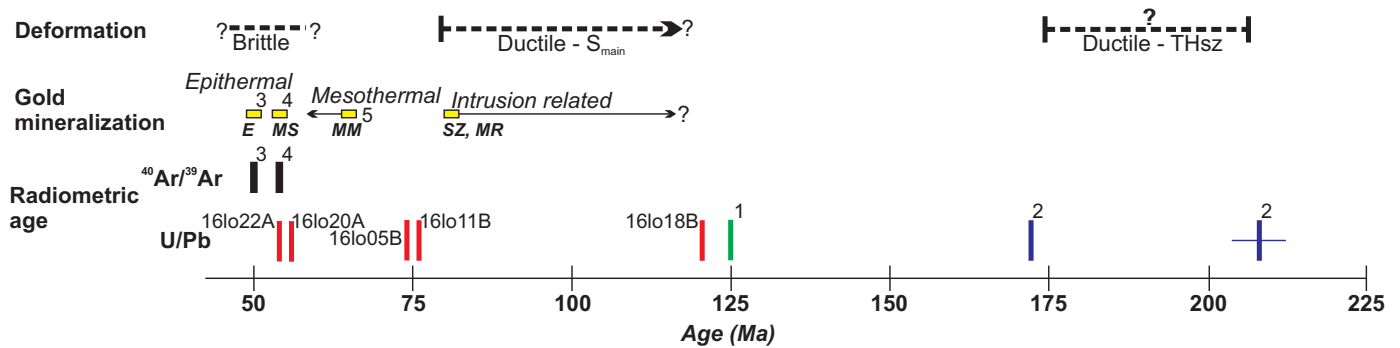


Fig. 8. Timeline summary of deformation and gold mineralization near the Llewellyn fault and Tally-Ho shear zone. Uranium-lead age constraints are from: this study (labelled by sample number); 1) Mihalynuk et al. (2003); 2) Tizzard et al. (2009). ⁴⁰Ar/³⁹Ar mica results are from: 3) Millonig et al. (2017) and 4) Love et al. (1998), and constrain the time of epithermal gold mineralization at Engineer Mine (E) and Mount Skukum Mine (MS). The suggested timing: of mesothermal gold mineralization at Mountana Mountain mines (MM) is from Hart and Pelletier (1989); of intrusion-related mineralization at the Skarn zone (SZ) is from this study; and of Middle ridge (MR) is from Mihalynuk et al. (2003). ?=uncertainty; S_{main}=main foliation along Llewellyn and Tally-Ho deformation corridor; THsz=Tally-Ho shear zone. See text for discussion.

possible that brittle movement began prior to ca. 56 Ma and the plutons overlap the initiation of brittle deformation along the Llewellyn fault.

Ductile deformation fabrics (foliations, folds, lineations) along the Llewellyn fault pre-date ca. 75 Ma. During this study, only one penetrative foliation (S_{main}) has been observed along the entire Llewellyn fault and Tally-Ho shear zone corridor. Although S_{main} is locally folded, no crenulation cleavage has been observed. The rhyolite southwest of Racine Lake, with an age of ca. 121 Ma (see above), pre-dates the development of S_{main}. However, two items need to be considered regarding the age of this rhyolite and the minimum timing of S_{main}. First, only two U-Pb zircon results are presented. Although two results would typically be considered insufficient, they may still be valid because both zircons are concordant and their ²⁰⁶Pb/²³⁸U ages overlap (Fig. 7e; Table 1). Also, the ca. 121 Ma age is not unique in the region. South of Bennett plateau, volcanic rocks underlying a mountain known as ‘Middle ridge’, yielded a U-Pb zircon age of ca. 125 Ma (Mihalynuk et al., 2003) for a unit originally mapped as Jurassic volcanic rocks (Fig. 2; unit lmJv on Mihalynuk et al., 1999). Furthermore, the Whitehorse plutonic complex is also ca. 120 Ma, although mostly preserved in Yukon (e.g., Hart and Radloff, 1990). Second, outcrops along the ridge are covered in grey lichen, making high-quality field observations difficult. The ridge is extensively overprinted by brittle faults, which are splays off the main Llewellyn fault. Although the rhyolite appears to share the same foliation as the surrounding rock units, it remains conceivable, but unlikely, that it post-dates ductile deformation and was imbricated with the foliated units during brittle faulting.

To further bracket the maximum age of S_{main}, the best location may be along the Tally-Ho shear zone, particularly at Mount Hodnett where S_{main} in the shear zone is parallel and probably formed at the same time as the foliation in the neighbouring granodiorite pluton (again mapped as Whitehorse plutonic complex; Hart and Radloff, 1990). Tizzard et al. (2009) preferred the explanation that the foliation is distinct and

related to a fault that juxtaposes the granodiorite and Tally-Ho shear zone. We collected a sample of this granodiorite in 2017 for U-Pb zircon dating. Should it yield a Jurassic or Triassic age, then development of S_{main} between 208 and 173 Ma may still hold (Tizzard et al., 2009). If the granodiorite is part of the Whitehorse plutonic suite, then the best interpretation is that S_{main} post-dates ca. 120 Ma. Based on the information at hand, we speculated that S_{main}, the only foliation preserved along the Llewellyn-Tally-Ho corridor, developed before ca. 75 Ma and potentially after ca. 120 Ma (Fig. 8).

4.2. Gold mineralization and deformation

A goal of this study was to test the apparent relationship between the various styles of gold mineralization that are related to both the ductile and brittle structures, as well as magmatism, along the Llewellyn fault (Fig. 2). The gold mineralization styles range from epithermal to mesothermal to intrusion-related (see Section 2). The orogenic gold deposit model typically relates a crustal continuum of gold deposits to first-order crustal breaks and synchronous magmatism (e.g., Goldfarb et al., 2005; Dubé and Gosselin, 2007). Therefore, the question arises as to whether the gold mineralization styles along the Llewellyn deformation corridor are interrelated, and if so are they part of an orogenic-style mineralizing system? In this model, the ductile and brittle deformation need to be contemporaneous, and gold mineralization is forming synchronously at various depths in the crust (e.g., Goldfarb et al., 2005).

The hypothesis fails because the field relationships and U-Pb zircon geochronology demonstrate a time gap of at least ca. 20 Ma between ductile and brittle deformation (Fig. 8). The older ductile deformation is defined by a regional foliation (S_{main}) in the Stikine terrane rocks (Stuhini, Lewes River, and Laberge groups) and possibly the Boundary Ranges metamorphic complex. The S_{main} is older than ca. 75 Ma (Figs. 7 and 8). Therefore intrusion-related gold mineralization that formed before or during the early-ductile phase of deformation, such

as in the Skarn zone at Bennett plateau and perhaps Middle ridge (Mihalynuk et al., 2003), predates ca. 75 Ma. According to our new U-Pb zircon age from a rhyolite west of Racine Lake, and speculations regarding fabric development along the Tally-Ho shear zone (Section 2.1.2.), some of the ductile deformation may post-date ca. 120 Ma. If intrusion-related gold mineralization, such as that at Bennett plateau and possibly Middle ridge developed during the time period 120 to 75 Ma, then this mineralization falls within the time-frame and style typical of the Tintina gold belt in Yukon and Alaska (e.g., Hart, 2007).

The epithermal-style gold mineralization, such as at Engineer Mine and Mount Skukum, have been dated at ca. 55 to 50 Ma and are clearly related to brittle deformation (Fig. 8; Love, 1990; Love et al., 1998; Millonig et al., 2017; Ootes et al., 2017). This time frame of brittle deformation corresponds to similar Cordillera-scale faults (e.g., Gabrielse et al., 2006). What remains unresolved is the absolute timing of mineralization at Montana Mountain (Yukon), which is considered mesothermal, post-dates Upper Cretaceous volcanic rocks, and has been suggested to be younger than Paleocene (Fig. 8; Roots, 1981; Walton, 1986; Hart and Pelletier, 1989). An attempt to date mineralization using the Re-Os arsenopyrite method was unsuccessful due to insufficient Re in the arsenopyrite (P. Mercier-Langevin, personal communication, 2017).

5. Conclusions

The Llewellyn fault overprints early ductile fabrics in British Columbia and the Tally-Ho shear zone, Yukon. Epithermal gold mineralization at the past-producing Mount Skukum and Engineer mines are related to this brittle deformation, and field and radiometric ages indicate that deformation and gold mineralization was between ca. 56 and 50 Ma (e.g., Love, 1990; Love et al., 1998; Millonig et al., 2017; Ootes et al., 2017). The brittle faults overprint an older ductile deformation history along the Llewellyn fault and Tally-Ho shear zone corridor. Previous work suggested the Tally-Ho shear zone developed between 208 and 173 Ma (Tizzard et al., 2009). Observations from this study indicate that the Tally-Ho shear zone contains only one fabric (S_{main}), and that this fabric is also in a neighbouring granodiorite pluton, previously considered part of the Whitehorse plutonic complex (ca. 120 Ma; Hart and Radloff, 1990). A rhyolite along the Llewellyn fault contains S_{main} . Based on our field and geochronologic data, we tentatively conclude that S_{main} developed after 120 Ma. Two granodiorite intrusions post-date the ductile deformation and yield U-Pb zircon crystallization ages of ca. 76 and 74 Ma. These new results indicate that the ductile deformation occurred before ca. 75 Ma. Intrusion-related gold mineralization, for example at the Skarn zone and possibly at Middle ridge (Mihalynuk et al., 2003; Wark, 2012), are deformed and pre-date 75 Ma. If these intrusion-related gold mineralizing systems developed between 120 and 75 Ma, then they may share characteristics with the Tintina gold belt in Yukon and Alaska.

This study further indicates that the Llewellyn fault extends into Yukon and crosscuts the Tally-Ho shear zone, and that this corridor shares the same early ductile deformation history (Hart and Radloff, 1990; Mihalynuk et al., 1999). A ca. 20 Ma time-gap between early and late deformation (Fig. 8) shows that gold mineralization associated with the ductile fabrics and with the brittle structures formed at different times, and therefore are related to distinct tectonic events.

Acknowledgments

This study complements, and is integrated with, a Geological Survey of Canada Targeted Geoscience Initiative research project, in collaboration with the Yukon Geological Survey. We thank BC Gold Corp. (Engineer Mine now owned by Blind Creek Resources), Troymet Exploration Corp., and Terralogic Exploration Inc. for access to properties and data. The study benefited from field assistant J. Elliott (2016, University of Victoria) and field visits and discussions with S. Casselman (Yukon Geological Survey) and S. Rowins and A. Hickin (British Columbia Geological Survey). Helicopter support was provided by Capital Helicopters, (Whitehorse, YT) and Discovery Helicopters (Atlin, BC). The U-Pb zircon work was at the University of British Columbia; H. Lin conducted mineral separation and assisted with mass spectrometry and T. Ockerman performed activities in the clean lab. Constructive and thoughtful reviews by N. Pinet and L. Aspler improved the clarity of the paper. This is NRCan Contribution number 20170305.

References cited

- Castonguay, S., Ootes, L., Mercier-Langevin, P., Rowins, S., and Devine, F., 2017. Orogenic gold along Cordilleran faults; key characteristics and analogies between Phanerozoic and Archean settings. In: Rogers, R., (Ed.), Targeted Geoscience Initiative-2016 Report of Activities, Geological Survey of Canada, Open File 8199, pp. 35-37.
- Crowley, J.L., Schoene, B. and Bowring, S.A., 2007. U-Pb dating of zircon in the Bishop Tuff at the millennial scale. *Geology*, 35, 1123-1126.
- Doherty, R.A. and Hart, C.J.R., 1988. Preliminary geology of Fenwick Creek (105D/3) and Alligator Lake (105D/6) map areas. Yukon Geological Survey, Open File 1988-2, 2 maps, 1:50,000 scale.
- Dubé, B., and Gosselin, P. 2007. Greenstone-hosted quartz-carbonate vein deposits. In: Goodfellow, W.D., (Ed.), Mineral Deposits of Canada: A Synthesis of Major Deposit-Types, District Metallogeny, the Evolution of Geological Provinces, and Exploration Methods. Geological Association of Canada, Mineral Deposits Division, Special Publication No. 5, pp. 49-73.
- Gabrielse, H., Murphy, D.C., and Mortensen, J.K., 2006. Cretaceous and Cenozoic dextral orogen-parallel displacements, magmatism, and paleogeography, north-central Canadian Cordillera. In: Haggart, J.W., Enkin, R.J. and Monger, J.W.H., (Eds.), Paleogeography of the North American Cordillera: Evidence For and Against Large-Scale Displacements. Geological Association of Canada, Special Paper 46, pp. 255-276.
- Gerstenberger, H., and Haase, G., 1997. A highly effective emitter substance for mass spectrometric Pb isotopic ratio determinations. *Chemical Geology*, 136, 309-312.
- Goldfarb, R.J., Baker, T., Dubé, B., Groves, D.I., Hart, C.J.R., and

- Gosselin, P., 2005. Distribution, character, and genesis of gold deposits in metamorphic terranes. In: J.W. Hedenquist, J.W., Thompson, J.F.H., Goldfarb, R.J., and Richards, J.P., (Eds.), *Economic Geology 100th Anniversary Volume*, pp. 407-450.
- Hart, C.J.R., 2007. Reduced intrusion-related gold-systems. In: Goodfellow, W.D., (Ed.), *Mineral Deposits of Canada: A Synthesis of Major Deposit-Types, District Metallogeny, the Evolution of Geological Provinces, and Exploration Methods*. Geological Association of Canada, Mineral Deposits Division, Special Publication No. 5, pp. 95-112.
- Hart, C.J.R., and Pelletier, K.S., 1989. Geology of Carcross (105D/2) and Part of Robinson (105D/7) Map Areas. Indian and Northern Affairs Canada, Yukon Geological Survey, Open File 1989-1, 84 p.
- Hart, C.J.R., and Radloff, J.K., 1990. Geology of Whitehorse, Alligator Lake, Fenwick Creek Carcross and part of Robinson map areas (105D/11, 6, 3, 2 & 7). Yukon Geological Survey, Open File 1990-4.
- Jaffey, A.H., Flynn, K.F., Glendenin, L.E., Bentley, W.C., and Essling, A.M., 1971. Precision measurement of half-lives and specific activities of ²³⁵U and ²³⁸U. *Physical Review C*, 4, 1889-1906.
- Love, D.A., 1990. Structural controls on veins of the Mount Skukum gold deposit, southwestern Yukon. Geological Survey of Canada, Paper 90-1E, pp. 337-346.
- Love, D.A., Clark, A.H., Hodgson, C.J., Mortensen, J.K., Archibald, D.A., and Farrar, E., 1998. The timing of adularia-sericite-type mineralization and alunite-kaolinite-type alteration, Mount Skukum epithermal gold deposit, Yukon Territory, Canada; ⁴⁰Ar - ³⁹Ar and U-Pb geochronology. *Economic Geology*, 93, 437-462.
- Ludwig, K.R., Isoplot 3.00, A Geochronological Toolkit for Microsoft Excel. University of California at Berkeley, kludwig@bgc.org.
- Mattinson, J.M., 2005. Zircon U-Pb chemical abrasion ("CA-TIMS") method: Combined annealing and multi-step partial dissolution analysis for improved precision and accuracy of zircon ages. *Chemical Geology*, 220, 47-66.
- Mihalynuk, M.G., Devine, F., and Friedman, R.M., 2003. Marksmen partnership: potential for shallow submarine VMS (Eskay-style) and intrusive-related gold mineralization, Tutshi Lake area. Ministry of Energy and Mines, British Columbia Geological Survey, GeoFile 2003-9, 1 poster.
- Mihalynuk, M.G., Smith, M., Hancock, K.D., Dudka, S.F., and Payne, J., 1994. Geology of the Tulsequah River and Glacier Creek Area (NTS 104K/12, 13). Ministry of Energy, Mines and Petroleum Resources, British Columbia Geological Survey Open File 1994-3, 3 sheets, 1:50,000 scale.
- Mihalynuk, M.G., Mountjoy, K.J., Currie, L.D., Smith, M.T., and Rouse, J.N., 1999. Geology and mineral resources of the Tagish Lake area (NTS 104M/8, 9, 10E, 15 and 104N/12W) northwestern British Columbia. Ministry of Employment and Investment, British Columbia Geological Survey Bulletin 105, 190 p.
- Millonig, L.J., Beinlich, A., Raudsepp, M., Devine, F., Archibald, D.A., Linnen, R.L., and Groat, L.A., 2017. The Engineer Mine, British Columbia: An example of epithermal Au-Ag mineralization with mixed alkaline and subalkaline characteristics. *Ore Geology Reviews*, 83, 235-257.
- Mundil, R., Ludwig, K. R., Metcalfe, I., and Renne, P. R., 2004. Age and timing of the Permian mass extinctions: U/Pb dating of closed-system zircons. *Science*, 305, 1760-1763.
- Nelson, J.L., Colpron, M., and Israel, S., 2013. The Cordillera of British Columbia, Yukon, and Alaska: Tectonics and metallogeny. In: Colpron, M., Bissing, T., Rusk, B.G., and Thompson, J.F.H., (Eds.), *Tectonics, Metallogeny, and Discovery: The North American Cordillera and similar accretionary settings*. Society of Economic Geologists, Special Publication 17, pp. 53-109.
- Ootes, L., Elliott, J.M., and Rowins, S.M., 2017. Testing the relationship between the Llewellyn fault, gold mineralization, and Eocene volcanism in northwest British Columbia: A preliminary report. In: *Geological Fieldwork 2016*, British Columbia Ministry of Energy and Mines, British Columbia Geological Survey Paper 2017-1, pp. 49-59.
- Roots, C.F., 1981. Geological setting of gold-silver veins on Montana Mountain. In: *Yukon Geology and Exploration 1979-80*, Indian and Northern Affairs Canada/Department of Indian and Northern Development: Exploration and Geological Services Division, pp. 116-122.
- Scoates, J.S., and Friedman, R.M., 2008. Precise age of the platinumiferous Merensky Reef, Bushveld Complex, South Africa, by the U-Pb ID-TIMS chemical abrasion technique. *Economic Geology*, 103, 465-471.
- Schmitz, M.D., and Schoene, B., 2007. Derivation of isotope ratios, errors, and error correlations for U-Pb geochronology using ²⁰⁵Pb-²³⁵U-(²³³U)-spiked isotope dilution thermal ionization mass spectrometric data. *Geochemistry, Geophysics, Geosystems*, 8, Q08006, doi:10.1029/2006GC001492.
- Stacey, J.S., and Kramers, J.D., 1975. Approximation of terrestrial lead isotopic evolution by a two-stage model. *Earth and Planetary Science Letters*, 26, 207-221.
- Thirlwall, M.F., 2000. Inter-laboratory and other errors in Pb isotope analyses investigated using a ²⁰⁷Pb-²⁰⁴Pb double spike. *Chemical Geology*, 163, 299-322.
- Tizzard, A.M., Johnston, S.T., and Heaman, L.M., 2009. Arc imbrication during thick-skinned collision within the northern Cordilleran accretionary orogen, Yukon, Canada. *Geological Society, London, Special Publications*, 318, 309-327.
- Walton, L., 1986. Textural characteristics of the Venus vein and implications for ore shoot distribution. In: *Yukon Geology Volume 1*, Exploration and Geological Services Division, Indian and Northern Affairs Canada, pp. 67-71.
- Wark, J.M., 2012. Technical Report, Golden Eagle Property. 43-101 Technical Report for Troymet Exploration Ltd., July 2012, 471 p. <https://www.troymet.com/projects/golden-eagle>.